Monthly Notices
of the
ROYAL ASTRONOMICAL SOCIETY

MNRAS **492,** L61–L65 (2020)
Advance Access publication 2019 November 04

doi:10.1093/mnrasl/slz167

Chemodynamical properties of the Anticentre Stream: a surviving disc fossil from a past satellite interaction

Chervin F. P. Laporte,[1]★† Vasily Belokurov,[2] Sergey E. Koposov,[2,3] Martin C. Smith[4] and Vanessa Hill[5]

[1]*Department of Physics and Astronomy, University of Victoria, 3800 Finnerty Road, Victoria, BC V8P 5C2, Canada*
[2]*Institute of Astronomy, University of Cambridge, Madingley Road, Cambridge CB3 0HA, UK*
[3]*McWilliams Center for Cosmology, Carnegie Mellon University, 5000 Forbes Ave, Pittsburgh, PA 15213, USA*
[4]*Key Laboratory for Research in Galaxies and Cosmology, Shanghai Astronomical Observatory, Chinese Academy of Sciences, 80 Nandan Road, Shanghai 200030, China*
[5]*Laboratoire Lagrange, Université Côte d'Azur, Observatoire de la Côte d'Azur, Boulevard de l'Observatoire, CS 34229, F-06304 Nice, France*

Accepted 2019 October 18. Received 2019 October 14; in original form 2019 July 22

ABSTRACT

Using *Gaia* second data release (DR2), we trace the Anticentre Stream (ACS) in various stellar populations across the sky and find that it is kinematically and spatially decoupled from the Monoceros Ring. Using stars from LAMOST and SEGUE, we show that the ACS is systematically more metal-poor than Monoceros by 0.1 dex with indications of a narrower metallicity spread. Furthermore, the ACS is predominantly populated of old stars (~ 10 Gyr), whereas Monoceros has a pronounced tail of younger stars ($6-10$ Gyr) as revealed by their cumulative age distributions. Put together, all of this evidence support predictions from simulations of the interaction of the Sagittarius dwarf with the Milky Way, which argue that the ACS is the remains of a tidal tail of the Galaxy excited during Sgr's first pericentric passage after it crossed the virial radius, whereas Monoceros consists of the composite stellar populations excited during the more extended phases of the interaction. Importantly, the ACS can be viewed as a stand-alone fossil of the chemical enrichment history of the Galactic disc.

Key words: Galaxy: abundances – Galaxy: disc – Galaxy: evolution – Galaxy: kinematics and dynamics – Galaxy: structure.

1 INTRODUCTION

Signs of vertical disc perturbations to the Milky Way (MW) disc have been known from the distribution of the neutral hydrogen gas since the 1950s (Burke 1957). In recent years, interest in disc quakes – particularly in the stellar component – has been reinvigorated with the discovery of spatial and kinematic North/South asymmetries around the solar neighbourhood (Widrow et al. 2012; Williams et al. 2013; Carlin et al. 2013; Carrillo et al. 2018; Schönrich & Dehnen 2018). As revealed by star count studies, these asymmetries take their most dramatic form in the outer edge of the Galaxy where the self-gravity of the disc is at its weakest. Amongst the various tributaries of the Galactic Anticentre, we note the Monoceros Ring (Newberg et al. 2002; Slater et al. 2014) and its substructured content, namely the Anticentre Stream (ACS) and Eastern Banded Structure (Grillmair 2006) that most visibly stand out in main-sequence (MS) and main-sequence turn-off (MSTO) star counts. Although initially thought to be part of the remains of a torn-apart accreted dwarf galaxy (Peñarrubia et al. 2005), recent theoretical (Gómez et al. 2016; Laporte et al. 2018; Laporte, Johnston & Tzanidakis 2019a) and observational studies favour an excited disc origin for these structures as supported by the kinematics (de Boer, Belokurov & Koposov 2018; Deason, Belokurov & Koposov 2018) and stellar populations (e.g. see Price-Whelan et al. 2015; Sheffield et al. 2018) with manifestly disc-like properties. Recently, Laporte et al. (2019a) suggested a re-interpretation of the ACS as the remnant of a tidal tail ('feather') excited by the Sgr dwarf galaxy shortly after virial radius crossing. A falsifiable predictions of this scenario is that the stellar populations of Monoceros and the ACS should show differences in metallicity and age distributions. In particular, because the ACS was excited through resonant processes with the reaction of the MW's dark matter halo with Sgr, it must have decoupled itself from the rest of the disc and should hold predominantly old stars and very few young ones. With the current synergy between legacy spectroscopic surveys (SEGUE, LAMOST, and APOGEE) and the second data release (DR2) from *Gaia*, it is now possible to dissect the Anticentre to much greater detail and test the tidal tail remnant hypothesis with chemistry and dynamics.

★ E-mail: cfpl@uvic.ca
† CITA National Fellow

This is the aim of the following contribution. In Section 2, we discuss our target selection and masks in the Monoceros Complex and cross-matches to the aforementioned spectroscopic surveys. In Section 3, we dissect the Monoceros Ring and ACS in metallicity, age, and abundance. We discuss our main findings and conclude in Sections 4 and 5.

2 TARGET SELECTION

For our study, we make use of the *Gaia* DR2 (GDR2) proper motions and parallaxes (Lindegren et al. 2018) to identify the likely ACS and Monoceros members. We correct magnitudes and colours (Evans et al. 2018) for extinction by using the Schlegel, Finkbeiner & Davis (1998) dust map and assuming $A_X = A_0 k_X$, where X designates the passband and k_X the first extinction coefficient of the relation used by Danielski et al. (2018) adapted to the *Gaia* passbands assuming that $A_0 = 3.1E(B - V)$ (Gaia Collaboration et al. 2018). To guide our initial spatial search, we begin by selecting the MS/MSTO by requiring $0.5 < \mathrm{BP} - \mathrm{RP} < 0.8$ and $18 < G_0 < 20$ and $\varpi < 0.1$. To define our sky selection, we convert the coordinates to a new system approximately aligned with the Anticentre by rotating the celestial equator to the great circle with a pole at $(l, b) = (325.00, 67.4722)$. The ACS and Monoceros stars are drawn from the spatial masks shown in Galactic coordinates in the top left panel of Fig. 1. Moreover, in the top right panel of the figure, using the red clump (RC) stars (selected with the cuts $15.5 < G_0 < 15.9$, $1.0 < \mathrm{BP} - \mathrm{RP} < 1.1$ and $\varpi < 0.1$), we demonstrate that the Monoceros Ring and the ACS not only have distinct spatial distributions but also differ kinematically. This is evidenced by the bifurcating pattern in (μ_l, μ_b) space for which we also present median proper motion tracks in magenta (blue) for the ACS (Monoceros) respectively. This two-horned structure confirms some of the earlier observations based on the *Gaia* DR1–Sloan Digital Sky Survey (SDSS) astrometric analysis of de Boer et al. (2018) that the ACS and Monoceros were decoupled.

We proceed by using GDR2 to identify high-fidelity candidate stars belonging to the ACS and the Monoceros regions. We make use of the parallax cut $\varpi < 0.1$ as well as the proper motion masks shown in Fig. 1. The two bottom rows of the figure give column-nornalized RC density in the space of μ_b and μ_l proper motions as a function of Galactic longitude l for Monoceros (ACS) in the left (right). The proper motion masks – highlighted by the magenta and blue boxes respectively – are chosen to include the highest density signal at each l. Fig. 2 presents colour-magnitude diagrams (CMDs) for both fields and only displays stars that have passed the proper motion and parallax cuts described above. Readily identifiable in the figure are several familiar stellar populations: MS/MSTO, RC, and red giant branch (RGB), thus confirming that our selection picks up bona-fide stars associated with the two individual well-defined structures. Moreover, note that the Hess diagram of the Monoceros Ring is *slightly* broader compared to the ACS, which signals a larger mix of metallicities and ages and possibly line-of-sight distances.

3 CHEMICAL AND AGE DECOMPOSITION OF MONOCEROS AND THE ACS

3.1 Metallicity distributions

The LAMOST DR4 survey (Luo et al. 2015) provides a good coverage of the Anticentre region, with a large number of spectra measured across both structures without a strong metallicity bias (see e.g. Yanny et al. 2009). SEGUE fares similarly well and has also the advantage of reaching down to the MS and the turn-off at larger distances. This is particularly advantageous to analyse differences in age distributions between Monoceros and the ACS for which the MSTO is sensitive to. Note however that SEGUE includes a subdominant target category (F subdwarfs) biased against more metal-rich stars. Furthermore, in order to avoid any source of confusion we only analyse stars in the range $115 < l < 175$ from our spatial and proper motion cuts defined in Introduction as these regions separate most clearly between the ACS and Monoceros fields both spatially and kinematically (see Fig. 1). Moreover, we select spectra with signal-to-noise ratios of S/N$\geq$10 for LAMOST an S/N$\geq$20 for SEGUE. Fig. 3 shows metallicity distributions for the likely Monoceros and the ACS members from our cross-matches with LAMOST and SEGUE. Although the numbers differ from one survey to another, both spectroscopic samples reveal similar systematic trends. The median metallicity of the ACS is consistently lower than that of Monoceros by some Δ[Fe/H] ~ 0.1 dex. Our results are consistent with those of Li et al. (2012)

3.2 Age distributions

To study the star formation histories of the two structures, we cross-match the candidate stars identified above with the catalogue of stellar ages computed by Sanders & Das (2018). Fig. 4 shows the cumulative age distributions for the ACS and Monoceros regions.[1] The difference between the two structures are remarkable, with the ACS being predominantly composed of older stars $\tau_{\mathrm{ACS}} > 10$ Gyr, whereas Monoceros possessing a more steady, gradual star formation history. We checked that there was no correlation between age and metallicity in our subset of Sanders & Das (2018) cross-matched stars and that the distances are consistent with the structures ($d \sim 10$ kpc). In the encounter scenario (see Laporte et al. 2019a), the ACS is a group of stars located in a tidal tail of the Galactic disc which gets decoupled from the rest of the disc and propelled to larger heights from mid-plane after first pericentric passage of a massive satellite (e.g. Sgr), whereas Monoceros consists of stellar populations in the flared and corrugated outer disc which was gradually built up through a succession of encounters, allowing it to replenish itself with younger stars as the star formation proceeded. Fig. 5 presents a spatial median age map of the Anticentre region. We find that the ACS is systematically older than the Monoceros Ring which hosts plenty of intermediate age stars (5–9 Gyr). Note a sharp age boundary between the two structures matching the location of the density transition (cf. Fig. 1).

3.3 APOGEE chemical abundances for the ACS and Monoceros

Despite its pencil-beam nature, the APOGEE survey (Majewski et al. 2017) covers parts of both the ACS and the Monoceros Ring. This allows us to acquire alpha-element abundances for our candidate stars through cross-matching catalogues. This gives us a few candidate stars which fall within the RGB/RC as shown in Fig. 2. In Fig. 6, we show the locations of our APOGEE cross-matched stars in the the space of ([Mg/Fe], [Fe/H]). Not surprisingly, these stars belong to the low-α sequence with $0 <$ [Mg/Fe] < 0.15 and low metallicity $-0.8 <$ [Fe/H] < 0.3, commonly known as the chemical 'thin disc', which confirms that the ACS and

[1]We have also checked that our results remain unchanged when focusing only on the MSTO stars, which would give the best age estimates compared to the RC and RGB.

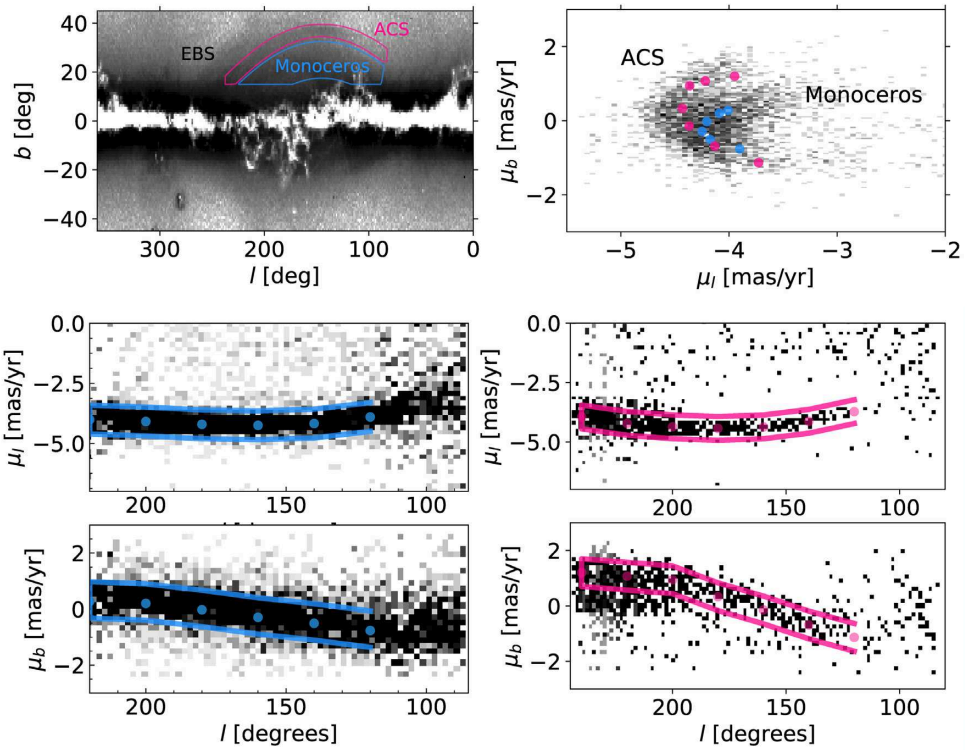

Figure 1. Top left: MS/MSTO map of the Anticentre in Galactic coordinates (l, b) with selected spatial footprints for the ACS and Monoceros Ring. ACS sits above the Monoceros Ring as a long collimated thin structure. Top right: latitudinal against longitudinal proper motions for RC stars. The median proper motion tracks for the ACS and Monoceros are shown by the magenta and blue dots. Middle right: normalized histogram for longitudinal proper motions μ_l as a function of l for 'ACS field' stars. Proper motion masks and median μ_l within them are shown in magenta. Middle left: normalized histogram for longitudinal proper motions μ_l as a function l for 'Monoceros field' stars. Proper motion masks and median μ_l within them are shown in blue. Bottom right: normalized histogram for latitudinal proper motions μ_b as a function of l for 'ACS field' stars. Note that this mask avoids the contamination from Monoceros situated below $\mu_b \sim 1 \mathrm{mas\,yr^{-1}}$ for $l > 200$ as the ACS and Monoceros overlaps spatially in those zones due to its reconnection with the mid-plane, yet show remarkably different kinematics. Proper motion masks and median μ_b within them are shown in magenta. Bottom left: normalized histogram for latitudinal proper motions μ_b as a function of l for 'Monoceros field' stars. Proper motion masks and median μ_b within them are shown in blue.

Monoceros Ring are not tidal debris from accretion events but truly extensions of the outer disc. This is not surprising as other/similar structures of the Anticentre have also recently been confirmed to be chemical thin-disc material through abundance measurements (e.g. see Bergemann et al. 2018) and stellar populations content (Price-Whelan et al. 2015; Sheffield et al. 2018), namely A13 (Sharma et al. 2010) and TriAnd (Rocha-Pinto et al. 2004). Our results from APOGEE are comparable with those of Hayes et al. (2018) who studied abundance of stars in TriAnd.

4 DISCUSSION

By using a combination of astrometric, photometric, and spectroscopic informations, we were able to dissect the Monoceros Ring and the ACS in the space of kinematics, metallicities, α-abundances, and ages. This allowed us to explore and confirm a falsifiable prediction for their respective formation mechanisms as presented in Laporte et al. (2019a), namely that the ACS is the remnant tidal tail of the MW disc which formed through a resonant interaction with a dwarf galaxy. The ACS was kicked up shortly after the dwarf's crossing of the Galaxy's virial radius during one of the first pericentric passages. The ACS excitation resulted in a strong decoupling from the Galactic mid-plane, leading to a sudden shutdown of star formation as compared to the rest of the disc. This yielded the observed striking difference in the cumulative age distributions between the Monoceros and the ACS.

We note that several structures in the outer disc have also been identified. These include the EBS (Grillmair 2006) and the more distant TriAnd clouds (Rocha-Pinto et al. 2004). A similar analysis could in principle be pursued, in particular for the TriAnd, which lies at a larger distance. This is particularly interesting as these structures may represent a fossil record of the formation history of the outer disc. Via modelling of such structures one can hope to time the impact events, putting strong constraints on the orbital mass-loss history of the Sgr dwarf galaxy. Our analysis argues that it may be possible to use chemistry and age dating important events in the lifetime of the Galactic disc. The decoupled nature of the structures analysed here – the ACS and the Monoceros – is of particular interest for chemodynamical models of the Galaxy (e.g. Chiappini, Matteucci & Gratton 1997; Schönrich & Binney 2009).

Given the disc nature of the ACS, and the relatively simple dynamics of 'feathers' (Laporte et al. 2019a), this structure may also be used for constraining the flattening of the Galactic potential at large radii, thus setting strong limits on alternative dark matter models or the existence of a dark disc (Read et al. 2008), however this is beyond the scope of this contribution and will be presented elsewhere.

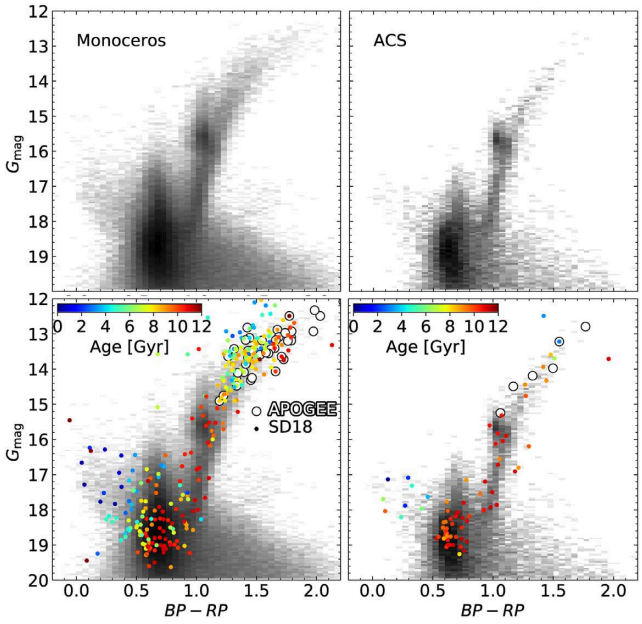

Figure 2. Top panels: CMDs for Monoceros and ACS fields (left- and right-hand panels, respectively). The kinematic and spatial selection picks up a well-defined RGB, RC all the way down to an MSTO/MS. The excess of blue stars may be a population of blue stragglers (BS). Bottom panels: stars identified in the Sanders & Das (2018) catalogue are shown as points colour-coded as a function of age. APOGEE cross-matched stars are shown as open white-filled black circles.

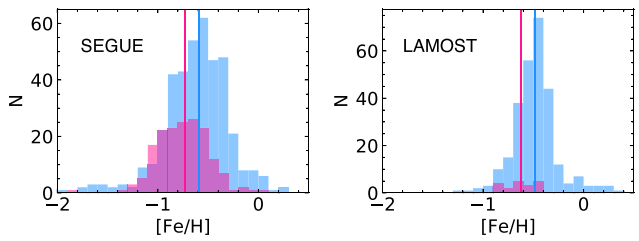

Figure 3. Left: metallicity distribution for stars cross-matched with SEGUE for the ACS and Monoceros Ring in magenta and blue, respectively. The median and spreads in metallicity ([Fe/H], σ[Fe/H]) are (−0.73, 0.26) and (−0.59, 0.32) for the ACS and Monoceros Ring, respectively. Right: metallicity distribution for stars cross-matched with sc LAMOST for the ACS and Monoceros Ring in magenta and blue, respectively. The median and spreads in metallicity ([Fe/H], σ[Fe/H]) are (−0.62, 0.14) and (−0.48, 0.22) for the ACS and Monoceros Ring, respectively.

5 CONCLUSION

In this work, we took full advantage of the synergy between GDR2, SEGUE, LAMOST, and APOGEE to show that:

(i) The ACS and Monoceros Ring are spatially and kinematically separate structures.

(ii) The ACS is on average more metal-poor than the Monoceros Ring, by ≥ 0.1 dex, with hints of a smaller spread in metallicity (though this could perhaps be accounted by distance spreads too).

(iii) The ACS and Monoceros Ring are both part of the chemically thin disc due to their low magnesium abundances, with $0.0 <$ [Mg/Fe] < 0.15.

(iv) The ACS has predominantly old stellar populations with 80 per cent having an age > 9 Gyr. This taken with its physical and kinematic decoupling from the rest of the disc, supports the hypothesis that this group of stars is a 'feather', i.e. the remnant of a tidal tail excited by a satellite encounter such as that with the Sgr dwarf described in Laporte et al. (2019a). In this model, the ACS is extracted from the disc during the dwarf's first passage after virial radius crossing, and no longer forms stars.

(v) The Monoceros Ring shows a steady cumulative age distribution suggesting that it belongs to main body of the disc which has been gradually flared and corrugated as a result of the multiple passages of Sgr and populated by stars of different ages as star formation continued.

As an outlook into the future, surveys such as WEAVE, SDSS V, 4MOST, and PSF will pave the road to a full coverage of the Anticentre. These surveys will not only provide radial velocities for a full characterization of the the phase-plane spiral in the outer disc as predicted by numerical models of the interaction of Sgr with the MW (Laporte et al. 2018, 2019b) but will also allow for a more detailed chemical dissection of the Anticentre. In particular, the

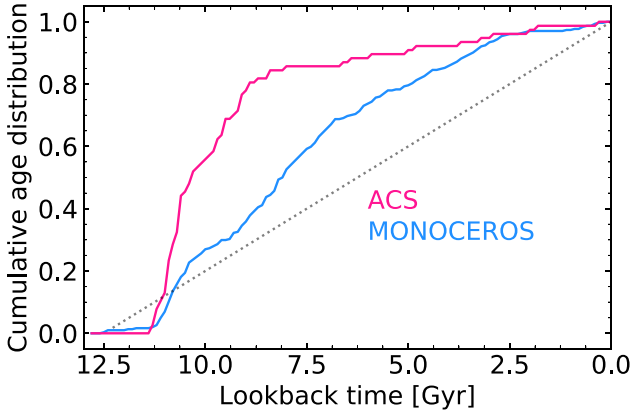

Figure 4. Cumulative age distribution of stars cross-matched with the Sanders & Das (2018) catalogue. The ACS shows a rapid increase in its cumulative distribution with about 80 per cent of the stars being older than ∼9 Gyr, whereas the Monoceros Ring shows a much more steady formation of stars. The black dotted lines shows the expectation for a uniform star formation rate.

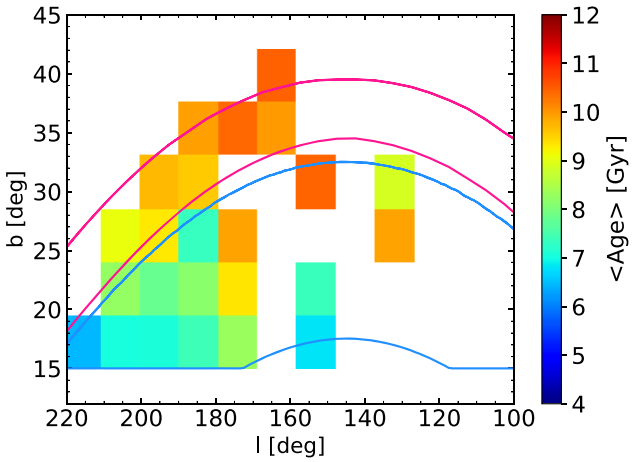

Figure 5. Spatial map of star median ages using MSTOs. Footprints of Monoceros and the ACS are shown in blue and magenta respectively.

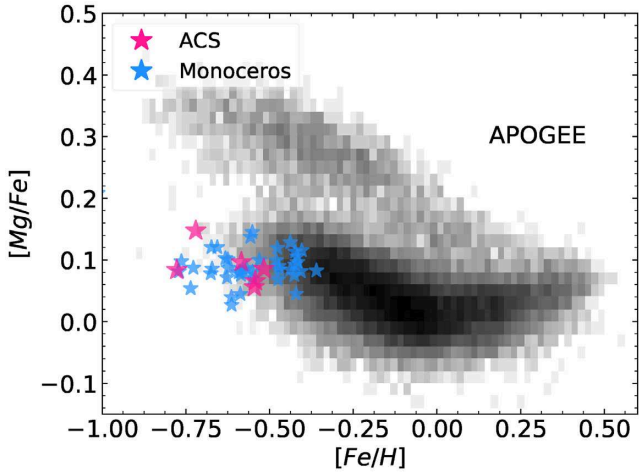

Figure 6. Magnesium abundance versus metallicity of stars in ACS and Monoceros within the proper motion masks defined in Introduction (magenta and blue star symbols respectively). Despite the pencil-beam nature of the APOGEE survey, a few stars associated with Monoceros and the ACS are picked up and show a clear low-α abundance sequence consistent with the chemical 'thin disc'. The full APOGEE disc [Mg/Fe] versus [Fe/H] map is displayed in grey scale for comparison.

latter will provide a window into the fossil record of the Galactic disc's formation.

ACKNOWLEDGEMENTS

This work has made use of data from the European Space Agency (ESA) mission *Gaia* (https://www.cosmos.esa.int/gaia), processed by the *Gaia* Data Processing and Analysis Consortium (DPAC, https://www.cosmos.esa.int/web/gaia/dpac/consortium). Funding for the DPAC has been provided by national institutions, in particular the institutions participating in the *Gaia* Multilateral Agreement. This paper made use of the Whole Sky Database (wsdb) created by S. Koposov and maintained at the Institute of Astronomy, Cambridge by SEK, VB, and W. Evans with financial support from the Science and Technology Facilities Council (STFC) and the European Research Council (ERC). CL and VB acknowledge support in part by KITP with support from the Heising–Simons Foundation and the National Science Foundation (grant no. NSF PHY-1748958). SK is partially supported by NSF grant AST-1813881 and Heising–Simons Foundation grant 2018-1030. MCS acknowledges financial support from the National Key Basic Research and Development Program of China (No. 2018YFA0404501) and National Science Foundation of China (NSFC grant 11673083). CL thanks Kathryn V. Johnston, Jorge Peñarrubia, Julio F. Navarro, and Isabel M. E. Santos-Santos for useful discussions.

REFERENCES

Bergemann M., et al., 2018, Nature, 555, 334,
Burke B. F., 1957, AJ, 62, 90
Carlin J. L., DeLaunay J., Newberg H. J., Deng L., Gole D., Grabowski K., 2013, ApJ, 777, L5
Carrillo I. et al., 2018, MNRAS, 475, 2679
Chiappini C., Matteucci F., Gratton R., 1997, ApJ, 477, 765
Danielski C., Babusiaux C., Ruiz-Dern L., Sartoretti P., Arenou F., 2018, A&A, 614, A19
de Boer T. J. L., Belokurov V., Koposov S. E., 2018, MNRAS, 473, 647
Deason A. J., Belokurov V., Koposov S. E., 2018, MNRAS, 473, 2428
Evans D. W. et al., 2018, A&A, 616, A4
Gaia Collaboration et al., 2018, A&A, 616, A10
Gómez F. A., White S. D. M., Grand R. J. J., Marinacci F., Springel V., Pakmor R., 2016, MNRAS, 465, 3446
Grillmair C. J., 2006, ApJ, 651, L29
Hayes C. R., Majewski S. R., Hasselquist S., Beaton R. L., Cunha K., Smith V. V., Price-Whelan A. M., 2018, ApJ, 859, L8
Laporte C. F. P., Johnston K. V., Gómez F. A., Garavito-Camargo N., Besla G., 2018, MNRAS, 481, 286
Laporte C. F. P., Johnston K. V., Tzanidakis A., 2019a, MNRAS, 483, 1427
Laporte C. F. P., Minchev I., Johnston K. V., Gómez F. A., 2019b, MNRAS, 485, 3134
Li J., Newberg H. J., Carlin J. L., Deng L., Newby M., Willett B. A., Xu Y., Luo Z., 2012, ApJ, 757, 151
Lindegren L., Hernández J., Bombrun A., Klioner S., Bastian U., Ramos-Lerate M., de Torres A., Steidelmüller H., 2018, A&A, 616, A2
Luo A. L. et al., 2015, Res. Astron. Astrophys., 15, 1095
Majewski S. R., Schiavon R. P., Frinchaboy P. M., Allende Prieto C., Barkhouser R., 2017, AJ, 154, 94
Newberg H. J., Yanny B., Rockosi C., Grebel E. K., Rix H.-W., Brinkmann J., 2002, ApJ, 569, 245
Peñarrubia J., Martínez-Delgado D., Rix H. W., Gómez-Flechoso M. A., 2005, ApJ, 626, 128
Price-Whelan A. M., Johnston K. V., Sheffield A. A., Laporte C. F. P., Sesar B., 2015, MNRAS, 452, 676
Read J. I., Lake G., Agertz O., Debattista V. P., 2008, MNRAS, 389, 1041
Rocha-Pinto H. J., Majewski S. R., Skrutskie M. F., Crane J. D., Patterson R. J., 2004, ApJ, 615, 732
Sanders J. L., Das P., 2018, MNRAS, 481, 4093
Schlegel D. J., Finkbeiner D. P., Davis M., 1998, ApJ, 500, 525
Schönrich R., Binney J., 2009, MNRAS, 396, 203
Schönrich R., Dehnen W., 2018, MNRAS, 478, 3809
Sharma S., Johnston K. V., Majewski S. R., Muñoz R. R., Carlberg J. K., Bullock J., 2010, ApJ, 722, 750
Sheffield A. A., Price-Whelan A. M., Tzanidakis A., Johnston K. V., Laporte C. F. P., Sesar B., 2018, ApJ, 854, 47
Slater C. T., Bell E. F., Schlafly E. F., Morganson E., Martin N. F., Rix H.-W., Peñarrubia J., 2014, ApJ, 791, 9
Widrow L. M., Gardner S., Yanny B., Dodelson S., Chen H.-Y., 2012, ApJ, 750, L41
Williams M. E. K., Steinmetz M., Binney J., Siebert A., Enke H., Famaey B., 2013, MNRAS, 436, 101
Yanny B., Rockosi C., Newberg H. J., Knapp G. R., Adelman-McCarthy J. K., Alcorn B., 2009, AJ, 137, 4377

This paper has been typeset from a TEX/LATEX file prepared by the author.